



Seismic Response of Structures with Underground Storeys

Principal Investigator

M. Hesham El Naggar, Ph. D, P. Eng.

Associate Professor

Department of Civil & Environmental Engineering

The University of Western Ontario

January 2003

ICLR Research
Paper Series – No. 26

ISBN 0-9732213-4-8

The Institute for Catastrophic Loss Reduction (ICLR) was established in 1998 with the mission to reduce the loss of life and property caused by severe weather and earthquakes through the identification and support of sustained actions to improve society's capacity to adapt to, anticipate, mitigate, withstand and recover from natural disasters.

For Further Information, please contact:
Institute for Catastrophic Loss Reduction
151 Yonge Street, Suite 1800
Toronto, Ontario, Canada M5C 2W7
Telephone: (416) 362-6112 ext 352
Fax: (416) 361-5952
E-mail: info@iclr.org www.iclr.org

The opinions expressed in this paper are those of the authors and not necessarily those of the Institute for Catastrophic Loss Reduction.

This material may be copied for purposes related to the document as long as the authors and copyright holders are recognized.

BRIEF SUMMARY AND ACHIEVEMENTS

The objective of the research is to investigate the effect of the interaction between basements and the surrounding soil medium on the estimated earthquake forces and deformations, for a variety of building types. To achieve this objective, the methodology involves the computer modeling of different buildings supported by different foundation systems. The computer model involves three-dimensional dynamic analysis of the combined superstructure and its foundation.

The first part of the study involved the analysis of the seismic response of tall slender R/C towers supported on flexible foundations. A new hybrid analysis was developed to model the nonlinear behaviour of the soil underneath the structure. A three dimensional finite element model was developed to represent the superstructure. The effect of the foundation flexibility on the seismic response of the tower was evaluated in terms of total displacements at the tip of the tower and the base forces (base bending moment and base shear). It was found that the foundation flexibility has a significant effect on the tower response to earthquake loading. The results showed that the soil-structure interaction could have a detrimental effect on tall structures contrary to what is postulated in design codes.

The foundation rocking behaviour could greatly contribute to the response of the supported structure to seismic loading, and in some cases it may become the governing factor when choosing a retrofitting scheme. In the second part of the study, analytical equations for the moment-rotation response of a rigid foundation are presented. An equation is derived for the uplift-yield condition and is combined with equations for uplift-only and yield-only conditions to enable the definition of the entire static moment-rotation response. The results obtained from the developed model show that the inverse of the factor of safety, χ , has a significant effect on the moment-rotation curve. The value of $\chi = 0.5$ not only determines whether uplift or yield occurs first but also defines the condition of the maximum moment-rotation response of the footing. The computed moment-rotation response agreed well with experimental results found in the literature, as well as the recommended NEHRP guidelines based on the FEMA 273/274 for the foundation moment-rotation. Three-dimensional finite element models are being developed for the seismic response analyses of multistory buildings. The soil model will be incorporated in the structural model and the global model will be used in the analysis.

Keywords: Seismic, soil-structure interaction, basement walls, rocking

TABLE OF CONTENTS

RESEARCH METHODOLOGY

PART I: SEISMIC RESPONSE OF TALL SLENDER STRUCTURES

I.1. Introduction

I.2. Concepts Of Proposed Approach

I.3. Equation of Motion

I.4. Ground Acceleration Motion

I.5. Solving The Equations

I. 6. Numerical Example

PART II: ANALYTICAL MOMENT-ROTATION CURVES FOR RIGID FOUNDATIONS

II.1 Introduction

II.2 Derivation of State Equations

II.3 Soil Yield and Foundation Uplift Condition

II.4 Properties of Moment-Rotation Curves

II.5 Discussion

II.6 Comparison with Experimental Results

II.6.1 TRISEE experiment

II.6.2 Comparison with TRISEE experiment

UTILITY OF RESEARCH RESULTS FOR THE INSURANCE INDUSTRY

CONCLUSIONS

ACKNOWLEDGEMENT

REFERENCES

List of Figures

- Figure I.1 Soil-structure system
- Figure I.2 Proposed model for soil-structure system
- Figure I.3 Milad TV-Tower, Tehran, Iran
- Figure I.4 Calculated time histories of bending moment at the base of the tower for site A with silty sand soil
- Figure II.1 Stresses and displacements for different footing states
- Figure II.2 Schematic of different states of moment-rotation response (after FEMA 273/274)
- Figure II.3 Computed moment-rotation curves for $c = 0.2$ a) for small y ; b) large y
- Figure II.4 Computed moment-rotation curves for different values of c for $y = 200$
- Figure II.5 Computed moment-rotation curves showing points of change of state
- Figure II.6 Load-deformation results from TRISEE experiments: a) load-deformation curves for HD tests; b) load-deformation curves for LD tests
- Figure II.7 Comparison between predicted and experimental moment-rotation curves

List of Tables

- Table I.1 Initial soil properties for free-field response
- Table I.2 Final soil properties for free-field response

RESEARCH METHODOLOGY

The seismic response of buildings with basement walls is a complicated phenomenon and is affected by several factors. The research reported here investigated two of the factors that influence the seismic response of buildings with basement walls in two parallel and independent studies. The first study was focused on the effects of soil-structure interaction (SSI) on the seismic response of tall structures. The second study was focused on the rocking response of rigid foundation. The following sections describe the methodology and findings of both studies.

PART I: SEISMIC RESPONSE OF TALL SLENDER STRUCTURES

I.1. Introduction

Numerical methods used for dynamic *SSI* can be classified into direct and substructure methods. The computational effort required for the direct analysis is high, rendering the procedure computationally inefficient for regular design applications. The substructure approach is computationally more efficient. This method divides the system into two subsystems, a superstructure that may include a portion of non-linear soil around the foundation (near-field) and a substructure that includes the unbounded soil around the superstructure (far-field). The subsystems are connected by a general soil-structure interface (Fig. I.1).

The consistent infinitesimal finite-element cell (CIFECM) method (Wolf & Song 1996) is a new approach that combines the advantages of the boundary element method and finite element method. A new three-dimensional dynamic *SSI* model based on the substructure method is developed to analyze the seismic response of tall structures accounting for soil non-linearity. In this methodology, the supporting soil is decomposed to some concave bounded media, where most of the non-linearity occur (near-field), and the unbounded medium representing the far-field soil zone. The CIFECM is used to evaluate the unbounded soil's reaction on the soil-structure interface and to model the bounded media, while the structure is represented by the FEM. The proposed procedure is used to examine the effect of soil non-linearity on the dynamic soil-structure analysis of a TV-tower subjected to strong ground motions.

I.2. Concepts Of Proposed Approach

The main concept of the proposed approach stems from the cloning algorithm due to Wolf (1985). The cloning concept is employed to model the non-linear soil zone underneath the

foundation (near-field) as a series of bounded media and the linear soil zone far from the foundation (far-field) as an unbounded medium. Each non-linear bounded zone may be represented by a non-linear frame element. The non-linear properties of each non-linear frame element including its non-linear force-deformation relationships are obtained using the non-linear deformation load concept. The stiffness matrix of each non-linear frame element is obtained using the direct stiffness method in structural matrix analysis by applying a unit deformation corresponding to each vibration mode (called motion pattern). Different motion patterns corresponding to the degrees of freedom of the frame element are considered including: vertical, horizontal and rocking motion patterns at two ends of the non-linear bounded medium. The CIFECM is then used to calculate the static stiffness and mass matrices of the bounded medium corresponding to the proposed motion patterns.

The flexural elements representing the non-linear zone of soil may be idealized using an uniaxial element with six internal non-linear springs and dashpots corresponding to the axial and torsional deformations, two bending rotations and two shear displacements. The equivalent static force-deformation relationships for the non-linear springs are calculated assuming no residual displacements and adjusting the shear modulus, G and material damping ratios according to the strain level in the layers to account for soil non-linearity. The frequency-dependent nature of the foundation compliance is accounted for by evaluating the foundation compliance at the fundamental frequency of the SS system (Darbre 1990). The effect of the frequency dependence of foundation compliance on the total response of the SS system is small and can be ignored.

I.3. Equation of Motion

When considering seismic excitation only, the equations of motion of a total structure-soil system (Fig. I.1) can be written as

$$\begin{bmatrix} \mathbf{M}_{bb} & \mathbf{M}_{ib} \\ \mathbf{M}_{bi} & \mathbf{M}_{ii} \end{bmatrix} \begin{Bmatrix} \ddot{\mathbf{u}}_b^t \\ \ddot{\mathbf{u}}_i^t \end{Bmatrix} + \begin{bmatrix} \mathbf{C}_{bb} & \mathbf{C}_{bi} \\ \mathbf{C}_{ib} & \mathbf{C}_{ii} + \mathbf{C}_{ii}^g \end{bmatrix} \begin{Bmatrix} \dot{\mathbf{u}}_b^t \\ \dot{\mathbf{u}}_i^t \end{Bmatrix} + \begin{bmatrix} \mathbf{K}_{bb} & \mathbf{K}_{bi} \\ \mathbf{K}_{ib} & \mathbf{K}_{ii} + \mathbf{K}_{ii}^g \end{bmatrix} \begin{Bmatrix} \mathbf{u}_b^t \\ \mathbf{u}_i^t \end{Bmatrix} = \begin{Bmatrix} \mathbf{0} \\ \mathbf{R}_i(t) \end{Bmatrix} \quad (\text{I.1})$$

in which \mathbf{u}^t is the total displacement vector; \mathbf{M} , \mathbf{C} and \mathbf{K} are the mass, damping and stiffness matrices obtained by the finite-element formulation for the structure and by the CIFECM for the near-field soil as bounded media in the SS system. The subscript b denotes the degrees of freedom in the bounded zone of SS system including the structure and the soil; the subscript i represents those along the structure-soil interface between the bounded part and the unbounded

soil zone; the unbounded zone is represented by superscript g ; and $\mathbf{R}_i(t)$ is the earthquake force applied along the general structure-soil interface that can be calculated from the free-field responses, $\ddot{\mathbf{u}}_i^g$, as

$$\mathbf{R}_i(t) = - \begin{bmatrix} \mathbf{M}_{bb} & \mathbf{M}_{ib} \\ \mathbf{M}_{bi} & \mathbf{M}_{ii} \end{bmatrix} \mathbf{I} \ddot{\mathbf{u}}_i^g \quad (\text{I.2})$$

where $\ddot{\mathbf{u}}_i^g$ is the acceleration vector at the nodes i that lie on the structure-soil interface of the soil and \mathbf{I} is the unity vector. The governing differential equations of inertial motion for the proposed model for MDOF structures Fig. I.2) can then be written in the form of:

$$\begin{bmatrix} \mathbf{M}_{ss} & \mathbf{M}_{sf} & & & \\ \mathbf{M}_{fs} & \mathbf{M}_{ff} + \mathbf{M}_I^b & & & \mathbf{0} \\ & & \mathbf{M}_I^b + \mathbf{M}_{II}^b & & \\ & & & \mathbf{M}_{II}^b + \mathbf{M}_{III}^b & \\ & \text{sym.} & & & \mathbf{M}_{III}^b \end{bmatrix} \begin{Bmatrix} \ddot{\mathbf{u}}_s^t \\ \ddot{\mathbf{u}}_f^t \\ \ddot{\mathbf{u}}_I^t \\ \ddot{\mathbf{u}}_{II}^t \\ \ddot{\mathbf{u}}_i^t \end{Bmatrix} + \begin{bmatrix} \mathbf{C}_{ss} & \mathbf{C}_{sf} & & & \\ \mathbf{C}_{fs} & \mathbf{C}_{ff} + \mathbf{C}_I^b & -\mathbf{C}_I^b & & \mathbf{0} \\ & & \mathbf{C}_I^b + \mathbf{C}_{II}^b & -\mathbf{C}_{II}^b & \\ & & & \mathbf{C}_{II}^b + \mathbf{C}_{III}^b & -\mathbf{C}_{III}^b \\ & \text{sym.} & & & \mathbf{C}_{III}^b + \mathbf{C}^g \end{bmatrix} \begin{Bmatrix} \dot{\mathbf{u}}_s^t \\ \dot{\mathbf{u}}_f^t \\ \dot{\mathbf{u}}_I^t \\ \dot{\mathbf{u}}_{II}^t \\ \dot{\mathbf{u}}_i^t \end{Bmatrix} + \begin{bmatrix} \mathbf{K}_{ss} & \mathbf{K}_{sf} & & & \\ \mathbf{K}_{fs} & \mathbf{K}_{ff} + \mathbf{K}_I^b & -\mathbf{K}_I^b & & \mathbf{0} \\ & & \mathbf{K}_I^b + \mathbf{K}_{II}^b & -\mathbf{K}_{II}^b & \\ & & & \mathbf{K}_{II}^b + \mathbf{K}_{III}^b & -\mathbf{K}_{III}^b \\ & \text{sym.} & & & \mathbf{K}_{III}^b + \mathbf{K}^g \end{bmatrix} \begin{Bmatrix} \mathbf{u}_s^t \\ \mathbf{u}_f^t \\ \mathbf{u}_I^t \\ \mathbf{u}_{II}^t \\ \mathbf{u}_i^t \end{Bmatrix} = \begin{Bmatrix} \mathbf{0} \\ \mathbf{0} \\ \mathbf{0} \\ \mathbf{0} \\ \mathbf{R}_i \end{Bmatrix} \quad (\text{I.3})$$

where the subscripts f and s denote the nodes on the structure and first bounded medium interface and the remaining nodes of the structure, respectively (see Fig. I.1); and the subscripts I , II and III denote the bounded media numbers.

I.4. Ground Acceleration Motion

The ground motion at the structure-soil interface, called generalized scattered ground motion, $\{\ddot{u}_i^s\}$, can be calculated from the free-field motion, $\{\ddot{u}_i^f\}$, which does not depend on the bounded zone. The program SHAKE 91 may be used to perform the free-field analysis taking into account the effect of primary non-linear behaviour of the soil.

In Eq. I.2, the earthquake excitation is characterized by $\{\ddot{u}_i^s\}$, the motion at the nodes on the bounded and unbounded zones interface of SS system. This motion is different than what is usually obtained from the free-field analysis in which the excavated soil is assumed in. Therefore, it is necessary to calculate the scattered motion from the free-field motion, $\{\ddot{u}_i^f\}$, (Wolf 1985) which is determined by the free field site analysis.

I.5. Solving The Equations

The internal forces carried by the SS system are decomposed into two components and the dynamic equilibrium equations (Eq. I.3) can be rewritten as:

$$[?] \{\ddot{u}(t)\} + [C] \{\dot{u}(t)\} + [K]_l \{u(t)\} + \{P_n(t)\} = \begin{Bmatrix} \mathbf{0} \\ R_i(t) \end{Bmatrix} = \{P(t)\} \quad (I.4)$$

where $[M]$, $[C]$ and $[K]_l$ are the mass, proportional damping and stiffness matrices corresponding to the total degrees of freedom with the non-linear elements removed. $\{P_n(t)\} = [K]_n \{u(t)\}$ is the vector of forces in the non-linear elements including the viscous dampers and the non-linear springs and is computed by iteration at each time t in which $[K]_n$ is the stiffness matrix of the non-linear elements. Denoting the linear effective stiffness matrix for all the non-linear degrees of freedom $[K]_{eff}$, the equilibrium equation can be rewritten as

$$[?] \{\ddot{u}(t)\} + [C] \{\dot{u}(t)\} + [\tilde{K}] \{u(t)\} + \{P_n(t)\} = \{P(t)\} + [K]_{eff} \{u(t)\} \quad (I.5)$$

where $[\tilde{K}] = [K]_l + [K]_{eff}$.

The nodal displacements, $\{u(t)\}$, can be approximated by a linear combination of a set of linearly independent free-vibration eigenvectors in a classical mode-displacement superposition method, or load-dependent transformation vectors, $[\mathbf{F}]$, using the stiffness $[\tilde{K}]$, and the mass matrix $[M]$, as

$$u(t) = [\mathbf{F}] \{Y(t)\}; \quad \dot{u}(t) = [\mathbf{F}] \{\dot{Y}(t)\}; \quad \ddot{u}(t) = [\mathbf{F}] \{\ddot{Y}(t)\} \quad (\text{I.6})$$

where $\{Y(t)\}$ is the generalized coordinates obtained by solving the SDOF transformed systems of dynamic equilibrium equations. The eigenvectors, $[\mathbf{F}]$, can be computed from the undamped free-vibration eigen problem:

$$[K]_l [\mathbf{F}] = [\omega_l^2] [M] [\mathbf{F}] \quad (\text{I.7})$$

or alternatively, load-dependent transformation vectors (Ritz vectors) generated by an inverse iterative scheme from the fixed spatial distribution of the seismic load can be used for $[\mathbf{F}]$. The Ritz vectors have to satisfy the following equations:

$$[\mathbf{F}]^T [M] [\mathbf{F}] = \mathbf{I} \quad ; \quad [\mathbf{F}]^T [\tilde{K}] [\mathbf{F}] = \mathbf{O}^2 \quad ; \quad [\mathbf{F}]^T [C] [\mathbf{F}] = ? \quad (\text{I.8})$$

where \mathbf{I} is the identity matrix and \mathbf{O}^2 is a diagonal matrix of squared structural frequencies and in the case of standard proportional damping $?$ is a function of the damping ratio.

The non-linear modal forces of the non-linear elements are a function of corresponding nodal displacements that should be calculated in terms of local displacements. At any time, the deformation, $\{\mathbf{d}(t)\}$, in the local coordinate system of the non-linear elements can be expressed in terms of the nodal point displacements, $\{u(t)\}$, by a displacement transformation equation, i.e.

$$\{\mathbf{d}(t)\} = [A] \{u(t)\} \quad (\text{I.9})$$

The deformations in the non-linear elements can be expressed in terms of modal coordinates as

$$\{\mathbf{d}(t)\} = [A] [\mathbf{F}] \{Y(t)\} \quad (\text{I.10})$$

Given the deformation time histories of the non-linear elements and their basic non-linear properties, the non-linear modal forces are then calculated from

$$\{F_n(t)\} = ([A] [\mathbf{F}])^T (\{P_n(t)\} - [K]_{eff} \{u(t)\}) \quad (\text{I.11})$$

Therefore, the non-linear modal equations (7) have to be solved iteratively in each time step. Assuming that the linear and non-linear modal forces vary linearly during each time step, a mixed procedure as a combination of vector superposition method and incremental method,

which has been found to be efficient for systems with a small number of non-linear members (Wilson 1993) is used to solve the modal equations.

I. 6. Numerical Example

The procedure proposed in this study is used to investigate the dynamic non-linear soil-structure interaction of an actual TV-tower. The geometrical and geological data of the tower were made available to be used as an example for R/C tall slender structures. The TV-tower (Fig. I.3) is 435 m in height with a twelve-storey heavy observation building and a 120 m tube antenna. It has a flexible shallow foundation that consists of a mat footing and a transition structure between the shaft and the mat footing.

The structure is modeled by general shell and frame elements. Linear elastic material properties of $E = 40,000 \text{ MN/m}^2$ and $\nu \neq 0.2$ are used for the concrete. The steel antenna has material properties of $E = 2.1 \times 10^5 \text{ MN/m}^2$ and $\nu \neq 0.3$. The material damping ratios of five and three percent are used for the concrete and steel, respectively.

The seismic response of tall slender structures is largely influenced by the flexibility of the supporting soil medium (Halabian & El Naggar 2001). Therefore, in this study numerical models are set up for several possible combinations of the structural and soil models. Two different soil profiles (shown in Table I.1) are used to represent the practical soil stiffnesses. Both profiles have shear wave velocity that increases slightly with depth. For each soil profile, two different soil models are used to represent the effect of soil non-linearity in the near-field. For the purpose of analysis, the soil is assumed to be layered halfspace. Poisson's ratio equal to 0.3 is selected and the mass density of the two types of soil are assumed as 1850 kg/m^3 and 1750 kg/m^3 for silty sand and firm clay. For each of site profile and soil model possible combinations, an ensemble of two strong ground motion records, the N-S component of the 1940 El Centro Earthquake and N21E component of the 1952 Taft Earthquake are selected as the control free-field motions. The selected records are scaled to peak ground acceleration of 0.35g.

Using given earthquake excitations, the soil profiles described in Table I.1 and the corresponding low strain shear moduli and damping ratios as initial values, the free-field motions at the level of soil-structure interface (Fig. I.2) are obtained employing the described method and program SHAKE 91. The final effective strains (65 percent of the maximum octahedral shear

strains) and the associated shear moduli and damping ratios for both soil profiles (A and B) using the silty sand model due to the 1940 El Centro Earthquake are shown in Table I.2.

The properties of the bounded soil media (near-field) and unbounded soil medium (far-field) are chosen to be compatible with the final shear strain results obtained from the corresponding free-field site response analyses. The near-field soil is subdivided into two regions: region I in which the non-linear effects of soil are considered to be significant; and region II where non-linearity is expected to be small. The artificial interface separating the regions experiencing significant and small non-linear *SSI* is selected so that the dimension of region I is about one and half of the characteristic length of the embedment depth of the foundation. The impedance functions of the far-field soil (unbounded medium) were calculated at a frequency equal to the weighted average of the first three fundamental frequencies of the structure obtained from the analysis of the fixed–base case.

The seismic responses of the *SS* system for a combination of site A and the silty sandy soil model subjected to the 1948 El Centro Earthquake is calculated for these cases: fixed base, flexible base assuming linear soil behaviour and flexible base assuming non-linear soil behaviour. Figure I.4 shows the calculated time histories of bending moment at the base of the tower for the three cases. As it can be noted in this case, the effect of soil non-linearity is to decrease the base bending moment compared with the linear *SSI* case.

Comparing the results for the fixed-base and the linear near-field soil cases showed that the effect of the foundation was to decrease the base bending moment. This effect is more pronounced for softer soil. It is interesting to note that as the supporting soil gets stiffer the effect of soil non-linearity decreases. However, this effect depends on the excitation parameters.

The displacements at the top of the observation deck were also calculated. The following observations were made. First, the foundation flexibility has a significant effect on the tower response. Second, the soil non-linearity could increase or decrease the displacement response depending on the characteristics of the ground motion and the structure. Therefore, soil non-linearity should be considered for important structures as it may increase the displacements significantly. Third, unlike the base bending moment case, the effect of soil non-linearity on the displacement is more pronounced for stiffer soils.

PART II: ANALYTICAL MOMENT-ROTATION CURVES FOR RIGID FOUNDATIONS

II.1 Introduction

Foundation rocking contributes significantly to the seismic response of a foundation for both tall slender structures and medium-rise buildings (Meek, 1978). The rocking mode involves uplift of the foundation at one side and soil yielding at the other side of the foundation, and generally results in the permanent settlement of the footing. Many researchers have investigated the nonlinear foundation rocking action using rigorous finite element and boundary element models. However, finite element and boundary element solutions are not efficient for nonlinear time domain analysis since they require large computational time and effort, and thus are not practical for regular design purposes.

The static moment-rotation response forms an important part of the cyclic response of a footing, and thus, has to be accurately modeled when analyzing the seismic response of the supported structure. Siddharthan et al. (1992) presented a set of equations to evaluate the moment-rotation response for both uplift-only and yield-only conditions of a rigid foundation. The equations were derived in the context of a retaining wall foundation, and as such, they do not constitute all the necessary equations for the complete static response of a rigid foundation.

II.2 Derivation of State Equations

The following assumptions are made in the derivation of the state equations: the axial load is constant and acts at the center of the footing; the moment acts about the longitudinal axis of the footing and is computed about its center; and the length of the footing is one unit. Figure II.1 shows a schematic of the assumed stress and displacement conditions for various footing states. State 1 represents elastic conditions, state 2 represents the initial foundation uplift condition (uplift-only), state 3 represents the initial soil yield condition (yield-only) and state 4 represents the soil yield and foundation uplift condition. These states correspond to different segments of

the moment-rotation curve shown in Figure II.2 and are considered herein to derive the foundation moment-rotation response curve as follows.

II.3 Soil Yield and Foundation Uplift Condition

All previous work reported in the literature addresses either elastic condition, uplift-only and yield-only stress states. In this study, the state of stress of combined soil yield and foundation uplift is considered. An expression is derived to describe this state represented by segment 5 of the moment-rotation curve shown in Fig. II.2. Considering the kinematics of this stress state yields (refer to Fig. II.1d):

$$\mathbf{d}_0 = \mathbf{d}_{1x} + \mathbf{d}_{2x} = \mathbf{d}_{1u} + \mathbf{d}_{2u} = \mathbf{d}_{2v} \quad (\text{II.1})$$

Substituting into Eq. II.1 (from Fig. 3d), the following equations are obtained

$$q_x = k_v \mathbf{q} (B(1-\mathbf{h}) - x) \quad (\text{II.2a})$$

$$q_x = q_u + k_v \mathbf{q} (B\mathbf{x} - x) \quad (\text{II.2b})$$

Equating Eqs. II.2a and II.2b gives

$$(\mathbf{h} + \mathbf{x}) = 1 - \frac{q_u}{k_v \mathbf{q} B} \quad (\text{II.3})$$

Calculating forces and moments at the footing center gives

$$P = q_u B\mathbf{x} + \frac{k_v \mathbf{q} B^2}{2} (1 - (\mathbf{h} + \mathbf{x}))^2 \quad (\text{II.4a})$$

$$M = \frac{q_u B^2}{2} \mathbf{x}(\mathbf{x} - 1) + \frac{k_v \mathbf{q} B^3}{12} (1 - (\mathbf{h} + \mathbf{x}))^2 (-1 - 2\mathbf{h} + 4\mathbf{x}) \quad (\text{II.4b})$$

Substituting Eq. II.3 into Eqs. II.4a and b and rearranging, the equation for the moment- rotation curve for this condition can be derived as:

$$M = \frac{PB}{2} - \frac{P^2}{2q_u} - \frac{q_u^3}{24(k_v \mathbf{q})^2} \quad (\text{II.5})$$

the limiting case for $\theta \rightarrow \infty$ yields

$$\lim_{q \rightarrow \infty} M = \frac{PB}{2} - \frac{P^2}{2q_u} \quad (\text{II.6})$$

Equation II.6 gives the maximum moment capacity of the foundation, which can also be derived by considering the foundation equilibrium (statics) when a fully plastic stress block is assumed. Equation II.5 shows that the moment, M , is inversely proportional to the square of the rotation.

II.4 Properties of Moment-Rotation Curves

The equations derived above define the static moment-rotation response curve completely for any stress state. These equations are used to evaluate the response of different foundations under different loading conditions. To enable a comparison between different footings under different response conditions, non-dimensional variables (\mathbf{y} , \mathbf{c} , M_{qB}) are introduced as follows:

$$\mathbf{y} = \frac{k_v B}{q_u} \quad (\text{II.7a})$$

$$\mathbf{c} = \frac{P}{q_u B} \quad (\text{II.7b})$$

$$M_{qB} = \frac{M}{q_u B^2} \quad (\text{II.7c})$$

where \mathbf{y} is a soil property and represents the ratio of the soil stiffness to its strength; \mathbf{c} is the inverse of the foundation bearing capacity safety factor under vertical load, FS ; and M_{qB} is a normalized (non-dimensional) moment. Using these non-dimensional variables, the complete moment-rotation relation can be expressed as:

For $\mathbf{c} \leq \frac{1}{2}$

$$M_{qB} = \begin{cases} \frac{\mathbf{y}\mathbf{q}}{12} & 0 \leq \mathbf{q} \leq \frac{2\mathbf{c}}{\mathbf{y}} \\ \frac{\mathbf{c}}{6} \left(3 - 2\sqrt{\frac{2\mathbf{c}}{\mathbf{y}\mathbf{q}}} \right) & \frac{2\mathbf{c}}{\mathbf{y}} \leq \mathbf{q} \leq \frac{1}{2\mathbf{y}\mathbf{c}} \\ \frac{1}{2} (\mathbf{c} - \mathbf{c}^2) - \frac{1}{24\mathbf{y}^2\mathbf{q}^2} & \mathbf{q} \geq \frac{1}{2\mathbf{y}\mathbf{c}} \end{cases} \quad (\text{II.8a})$$

and for $\mathbf{c} \geq \frac{1}{2}$

$$M_{qB} = \begin{cases} \frac{yq}{12} & 0 \leq q \leq \frac{2(1-c)}{y} \\ \frac{(1-c)}{6} \left(3 - 2\sqrt{\frac{2(1-c)}{yq}} \right) & \frac{2(1-c)}{y} \leq q \leq \frac{1}{2y(1-c)} \\ \frac{1}{2}(c - c^2) - \frac{1}{24y^2q^2} & q \geq \frac{1}{2y(1-c)} \end{cases} \quad (\text{II8b})$$

Equations II.8a and II.8b show that the normalized moment, M_{qB} , is a function of only y and c . Figures II.3 and II.4 show the moment rotation response curves for a range of values of y and c .

Figure II.3 shows the moment-rotation curves for $c = 0.2$, and a range of practical values of y (50-1200). Small values of y (Figure II.3a) represent foundations supported on strong soils such as stiff clays and dense sand, where the soil strength is high compared to its stiffness. Such foundations will usually have a small width. On the other hand, large values of y (Figure II.3b) represent foundations of large width supported on a relatively low bearing capacity soil such as soft clay or loose sand. It is noted from Fig. II.3 that the rotational stiffness of the foundation (manifested by the slope of the moment-rotation curve) increases with an increase in y . The figure also reveals that the ultimate rotation decreases as y increases, almost linearly, i.e., the ultimate rotation decreased by an order of magnitude as y increased by an order of magnitude. It is worth mentioning here that Eurocode 7 (CEN, 1994) specifies 6 millirad (mrad) as the relative rotation to cause an ultimate limit state. From Fig. II.3, it can be observed that rotation of 6 mrad represents an elastic response for the case of $y = 50$ and represents a nonlinear response state for the case of $y = 1200$.

Figure I.4 shows the effect of c on the moment-rotation response of foundations with $y = 200$. The figure shows that the moment response increases as c increases until it reaches 0.5, and then declines as c continues to increase. The insert in Fig. II.4 shows that the maximum value of M_{qB} , which does not depend upon y , varies with c in a parabolic manner, and attains a maximum value of 0.125 at $c = 0.5$. This shows that $c = 0.5$ represents a limiting condition on the moment-rotation response of a spread rigid footing based on the Winkler soil model.

II.5 Discussion

The FEMA 273/274 documents and Siddharthan et al. (1992) state that the significance of c is that its value, above or below 0.5, indicates whether uplift of the foundation or yielding of the soil would occur first. However, the main significance of $c = 0.5$ is that it defines the maximum moment-rotation response possible as shown in Fig.II.4. This is further illustrated in Fig. II.5, which shows initiation of different stress states for different c values. For $c = 0.5$, the uplift-yield portion segment follows immediately after the elastic segment (point R). This shows that for this case ($c = 0.5$), a yield-only or uplift-only condition does not occur. On the other hand, uplift-only and yield-only conditions occur after the elastic condition at $q = 1$ mrad (point P) for $c = 0.1$ (e.g. foundations where conditions other than bearing capacity demands govern the design) and $c = 0.9$ (e.g. foundations of existing structures that need retrofitting because of increased loads as a result of code revisions or change in the use of structure), respectively. However, the yield-uplift condition occurs, but at a large rotation of $q = 25$ mrad (not shown on the graph). For $c = 0.3$ (typical foundation design) and $c = 0.7$ (foundation designed to mobilize its ultimate capacity under seismic conditions), uplift (for $c = 0.3$) and yield ($c = 0.7$) initiate at $q = 3$ mrad (point Q). The onset of the yield-uplift condition occurs at $\theta = 8$ mrad (point S). It can thus be concluded that as c approaches 0.5 from either side, the region where uplift-only or yield-only occurs shrinks and the region where yield and uplift occur expands. Based on this observation, three regions of moment-rotation responses can be postulated: uplift-dominant region; uplift-yield region; and yield-dominant region.

Based on the ensuing discussion, the following important observations can be made:

1. The moment-rotation curve included in the FEMA 273/274 documents (Fig. II.2) presents a seemingly different picture to some of the inferences drawn in this section. First, the curves for the initial uplift or initial yield conditions are shown as two separate curves (1-3-5-6 and 1-4-5-6, respectively), with the initial uplift curve lying above that for the initial yield. . This implies that for the same y value, a foundation design with $c < 0.5$ (which leads to initial uplift) would result in a larger moment response than the case where $c > 0.5$ (which leads to initial yield). However, both curves are similar and the moment-rotation response is rather influenced by the absolute difference between c and $c = 0.5$. Secondly, Fig. II.2 shows that

segment (5) of the curve, which represents the uplift-yield condition is asymptotic to the ultimate elastic condition, $M = PB/2$. This is incorrect, since no yielding occurs by definition (infinitely strong soil).

2. Siddharthan et al. (1992) stated that the rocking response could be grouped into either the initial uplift condition, or the initial yield condition. It has been shown that the ultimate moment for both conditions is the same if formulated in terms of c . The results presented herein show that based on the value of c , the moment-rotation response can rather be grouped into three categories based on dominating behaviour and not two categories based on the initiation of uplift or yield. The correct expression for the ultimate moment has also been derived.

II.6 Comparison with Experimental Results

The ability of the model developed in this study to evaluate the moment-rotation behaviour of a foundation is verified using available experimental results. The model developed is used to analyze the moment-rotation response of foundations subjected to rocking action in a laboratory testing program and the results are compared with the measured values.

The European Commission (EC) sponsored the project TRISEE (3D Site Effects of Soil-Foundation Interaction in Earthquake and Vibration Risk Evaluation), which included large-scale model testing to examine the response of rigid footings to dynamic loads. The results of these tests are of high quality and are readily available (Negro et al. 1998). Therefore, these tests are analyzed using the developed model and the results are compared with the measured values.

II.6.1 TRISEE experiment

The experiments involved a 1 m square footing model embedded to a depth of 1 m, in a 4.6 m by 4.6 m by 3 m deep sample of saturated Ticino sand. Ticino sand is a uniform coarse-to-medium silica sand. The properties of the sand are as follows: $D_{50} = 0.55$ mm; coefficient of uniformity, $C_u = 1.6$; specific gravity, $G_s = 2.684$; $e_{min} = 0.579$; and $e_{max} = 0.931$ (Jamiolkowski et al., 1999). Two series of tests were performed on the model foundation installed in two different soil samples with relative density of 45% (low density, LD) and 85% (high density, HD).

A vertical load of 100 kN and 300 kN was applied to the LD and HD samples, respectively, before the application of the horizontal cyclic loading phase. The imposed pressures of 100 kPa

and 300 kPa represent typical design pressures for foundations in medium to dense sands, where the design is usually governed by admissible settlement, not bearing capacity, requirements. The resulting static FS under vertical load only was found to be about 5 in both cases. The cyclic loading involved three phases: Phase I - the application of small-amplitude force-controlled cycles; Phase II - the application of a typical earthquake-like time history; and Phase III - sinusoidal displacement cycles of increasing amplitude. Only relevant sections of the results of the tests would be presented for comparison purposes. Further information on the experiments can be found in Negro et al. (1998, 2000), Pedretti (1998) and Jamiolkowski et al. (1999).

II.6.2 Comparison with TRISEE experiments

The load-deformation results obtained during the application of the static vertical load only (similar to a plate loading test) were used to back figure the soil subgrade. Figure II.6 shows the load-deformation results of the TRISEE experiments plotted in terms of e_a , along with the stiffness values for initial, secant and unload-reload loading conditions as evaluated from the test results. These values of the subgrade modulus are used in the developed Winkler model to calculate the moment-rocking response of the foundation and the results are compared with the measured response in Fig. II.7. It should be noted that the measured response represents the envelop of the loading cycles with gradually increasing peak amplitude (i.e. obtained by connecting the tips of the hysteretic loops). Lo Priesti et al. (1998) have noted that because of the different impact of plastic strains under different loading conditions, it is impossible to obtain the same backbone curve for both monotonic and cyclic loading. Figure II.7 shows that the results computed based on the unload-reload stiffness gives the best agreement with the experimental results. The initial stiffness is slightly underestimated, but the overall response is generally satisfactory. This is expected since cyclic loading represents an unload-reload action, and the unload-reload stiffness is more representative of the small-strain stiffness.

Soil nonlinearity and creep effects significantly influence the initial stiffness. For example, the experimental results for the LD specimen showed that the creep settlement accounted for about 40% of the observed settlement (Jamiolkowski et al., 1999). The response calculated based on the secant subgrade modulus is seriously overestimated (i.e. rocking stiffness is grossly underestimated) as shown in Fig. II.7. Although this is expected, the need for carefully

selecting the subgrade modulus values for either static or dynamic analysis of foundations is not fully appreciated in practice.

UTILITY OF RESEARCH RESULTS FOR THE INSURANCE INDUSTRY

The results of the research showed the significant effect of SSI on the seismic performance of tall structures. Therefore, it is necessary that proper SSI analysis be performed when designing tall structures to ensure satisfactory seismic performance of the structure. This will ensure that earthquake damage will be minimized.

CONCLUSIONS

The following conclusions were drawn:

- soil non-linearity could decrease or increase the lateral displacements for tall slender structures. This change should be considered in the analysis of tall slender structures where the P- Δ effect is one of the important design parameters.
- soil non-linearity may result in an increase or decrease in the base forces compared to those of the linear soil model case, depending on the type of structure, frequency of the input motion, and dynamic properties of the near-field soil. This shows that the SSI may not always have a favourable effect but could be detrimental in some cases.
- $c = 0.5$ represents the condition for the maximum moment response based on the Winkler soil model.
- The moment-rotation response is rather influenced by the absolute difference between c and $c = 0.5$, which dictates whether uplift of yield is dominant. Based on the value of c , the moment-rotation response can be grouped into three categories: uplift-dominant, uplift-yield and yield dominant.

ACKNOWLEDGEMENTS

This research was supported by a scholarship from the National Research Centre of Iran to the first author and a grant from the Institute of Catastrophic Loss Reduction, The University of Western Ontario, to the second author. The contribution of data from Yadman Sazeh Co. (the Management Consultant of the Milad TV-tower) is gratefully acknowledged. The models presented here and the results shown and discussed were part of the doctoral work of Dr. Amir

Halabian and Mr. Nii Allotey under the supervision of Dr. El Naggar at the University of Western Ontario.

REFERENCES

- ATC (1978). Tentative Provisions for the Development of Seismic Regulations for Buildings. *Applied Technology Council Report*, ATC 3-06, Palo Alto, California.
- Applied Technology Council (ATC) (1996). *ATC 40: The seismic evaluation and retrofit of concrete buildings*, Vol. I & II, Redwood, Palo Alto, California
- Building Seismic Safety Council (BSSC) (1997a). FEMA 273/274, *NEHRP guidelines for the seismic rehabilitation of buildings*, Vol.I–Guidelines, Vol.II – Commentary, Washington DC.
- Building Seismic Safety Council (BSSC) (1997b) FEMA 302/303, *NEHRP recommended provisions for seismic regulations for new buildings and other structures*, Vol. I – Guidelines, Vol. II – Commentary, Building Seismic Safety Council, Washington DC.
- CEN (1994). *Eurocode 7 – Geotechnical Design Part 1: General Rules*. European Committee for Standardization (CEN), Bruxelles, Belgium.
- Clough R.W. and Penzien, J.1993. *Dynamics of Structures*. McGraw-Hill Inc., New York.
- Darbre, G.R. 1990. Seismic analysis of non-linearly base-isolated soil-structure interacting reactor building by way of the hybrid frequency-time-domain procedure. *Earthquake Engineering and Structural Dynamics*, Vol. 16, pp.725-738.
- Halabian, A. M. and El Naggar, M. H. 2001. Effect of foundation flexibility on seismic response of reinforced concrete TV-towers. *Canadian J. of Civil Engineering*, Vol. 28(3), pp.465-481.
- Lo Priesti, D. C. F., Pallara, O., Cavallaro, A., Maugeri, M. (1998). Nonlinear stress-strain relations of soils for cyclic loading, Proc. of XI European Conf. on Earthquake Engineering, Paris, Balkema, Abstract volume CD-ROM, 187.
- Meek (1978). Dynamic response of tipping core buildings. *Earthquake Engineering and Structural Dynamics*, Vol. 6, pp. 453-454.
- Negro, P., Paolucci, R., Pedretti, S., Faccioli, E. (2000). Large scale soil-structure interaction experiments on sand under cyclic load. Paper No. 1191, *12th World Conference on Earthquake Engineering*, Auckland, New Zealand.

- Negro, P., Verzeletti, G., Molina, J., Pedretti, S., Lo Presti, D., Pedroni, S. (1998). Large-scale geotechnical experiments on soil-foundation interaction. *Special Publication No. I.98.73*, European Commission, Joint Research Center, Ispra, Italy.
- Pedretti, S. (1998). Nonlinear seismic soil-foundation interaction. *PhD Thesis*, Department of Structural Engineering, Politecnico di Milano, Italy.
- Schnabel, P. B., Lysmer, J. and Seed, H. B. 1972. SHAKE 91 – A computer program for earthquake response analysis of horizontally layered sites. *Report No. EERC 72-12*, Earthquake Engineering Research Center, University of California, Berkeley, California.
- Siddharthan, R. V., Ara, S., Norris, G. M. (1992). Simple rigid plastic model for seismic tilting of rigid walls. *Journal of Structural Engineering*, ASCE, Vol. 118, No. 2, pp. 469-487.
- Wolf, J. P. 1985. *Dynamic Soil-Structure Interaction*. Prentice-Hall, Englewood Cliffs, NJ.
- Wolf, J. P. and Song, C. 1996. *Finite-Element Modeling of Unbounded Media*. John Willey & Sons, New York.

Table I.1 Initial soil properties for free-field response

Layer	Thickness (m)	Initial shear Modulus (KN/m ²)		Initial damping ratio	
		Site A	Site B	Site A	Site B
1	3	81710	40850	0.02	0.02
2	2.25	90435	45215	0.02	0.02
3	2.25	123680	59440	0.02	0.02
4	2.50	158070	76640	0.02	0.02
5	2.50	167700	74245	0.02	0.02
6	5	164850	77650	0.02	0.02
7	5	188340	94171	0.02	0.02
8	20	233940	114580	0.02	0.02
9	20	281840	138530	0.02	0.02
10	halfspace			0.00	0.00

Table I.2 Final soil properties for free-field response

Layer	Thickness (m)	Effective strain		Final shear modulus (KN/m ²)	
		Site A	Site B	Site A	Site B
1	3	0.0169	0.0167	45630	22992
2	2.25	0.0800	0.0899	25890	11975
3	2.25	0.1023	0.1252	30302	13105
4	2.50	0.1113	0.1407	37200	15874
5	2.50	0.1545	0.3414	33233	8210
6	5	0.3068	0.5731	20746	6280
7	5	0.2868	0.5505	24348	7836
8	20	0.1421	0.4563	47584	10765
9	20	0.1179	0.5679	64225	11276
10	halfspace				

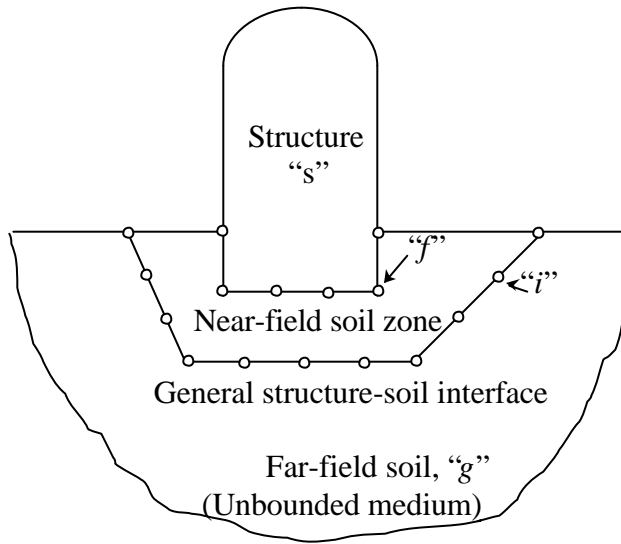


Figure I.1 Soil-structure system

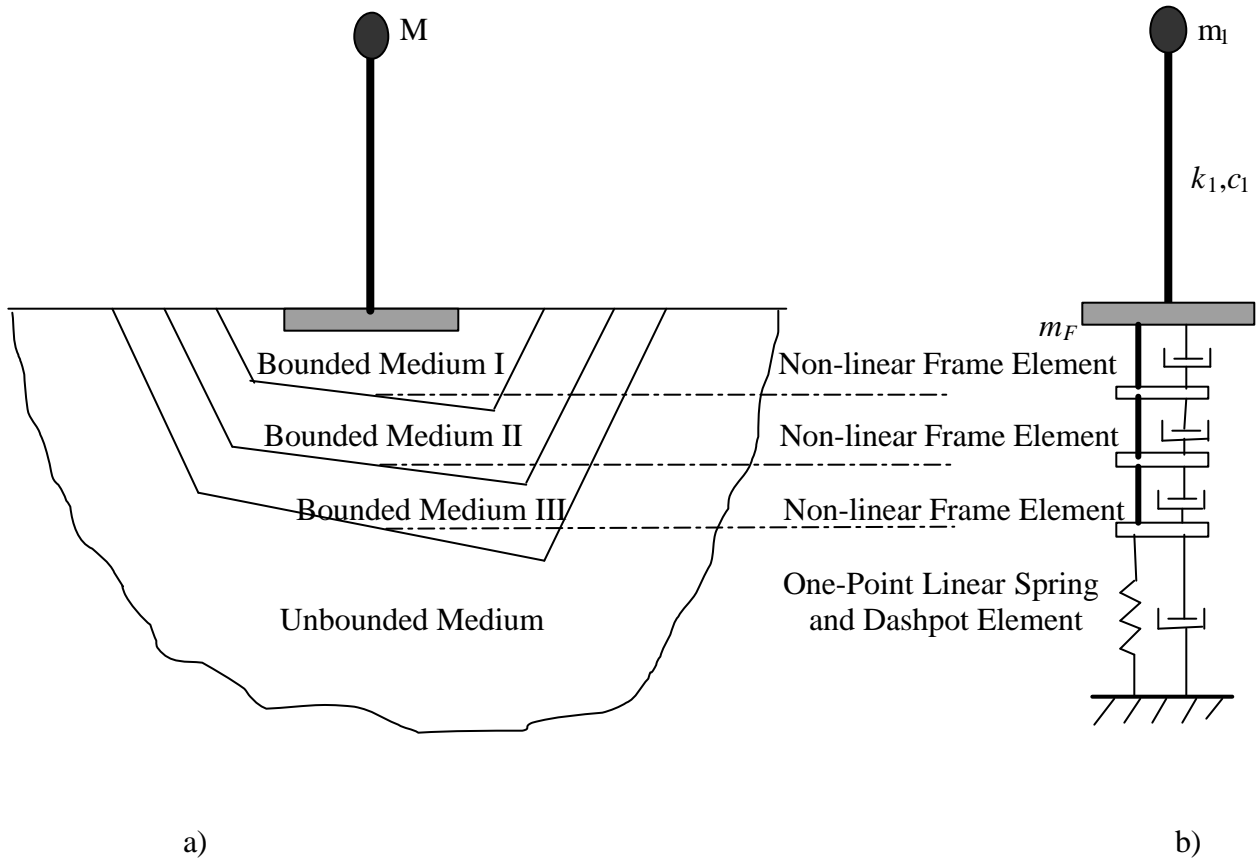


Figure I.2 Proposed model for soil-structure system

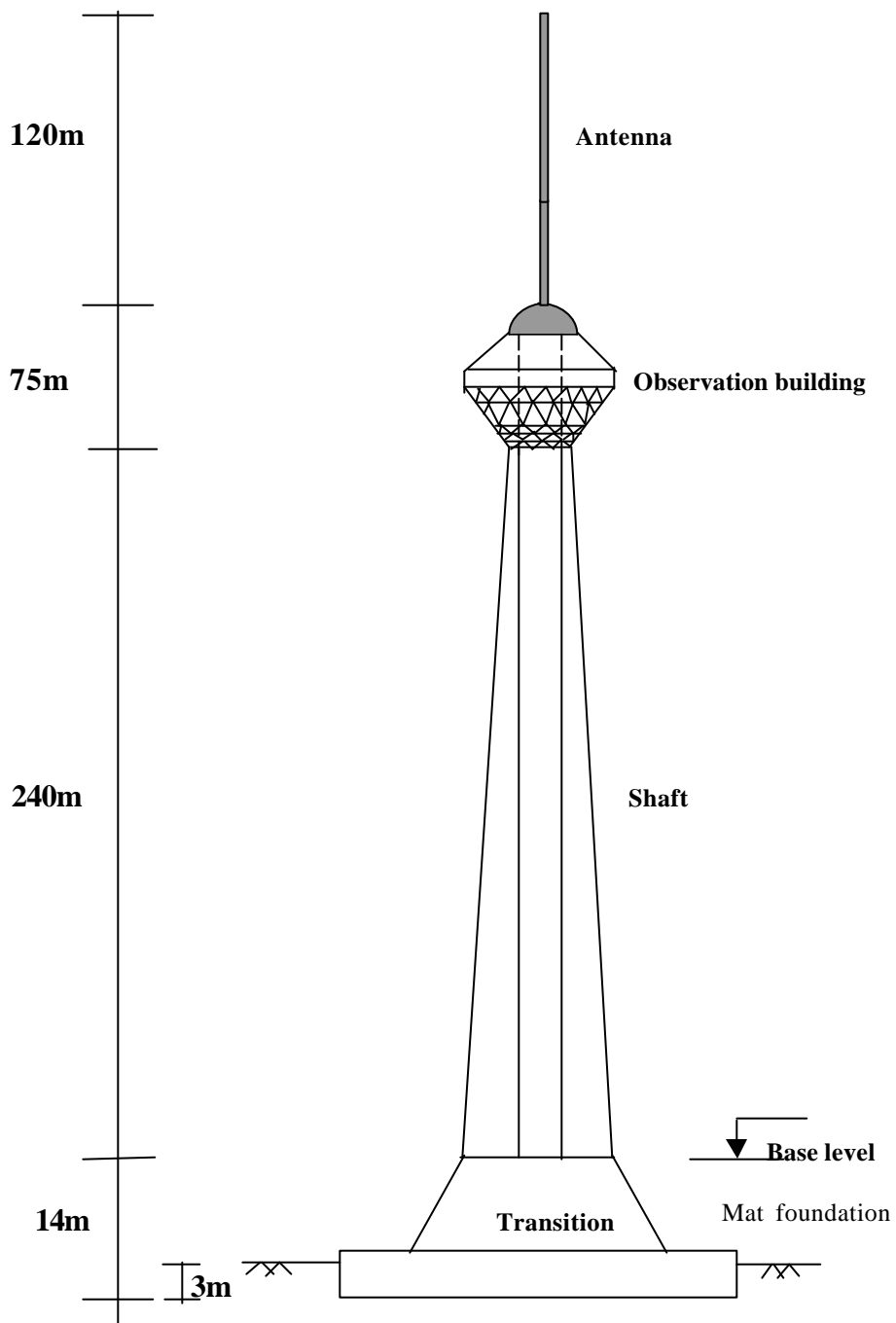
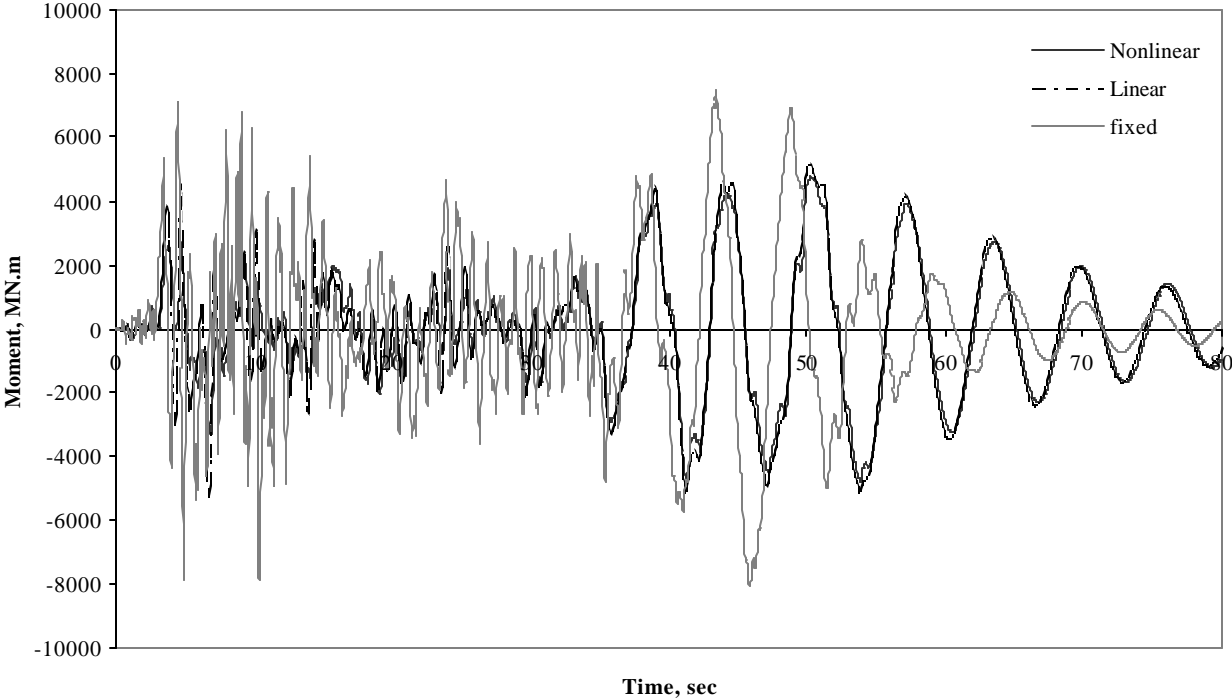


Figure I.3 TV-tower model

Figure I.4 Calculated time histories of bending moment at the base of the tower for site A with silty sand soil



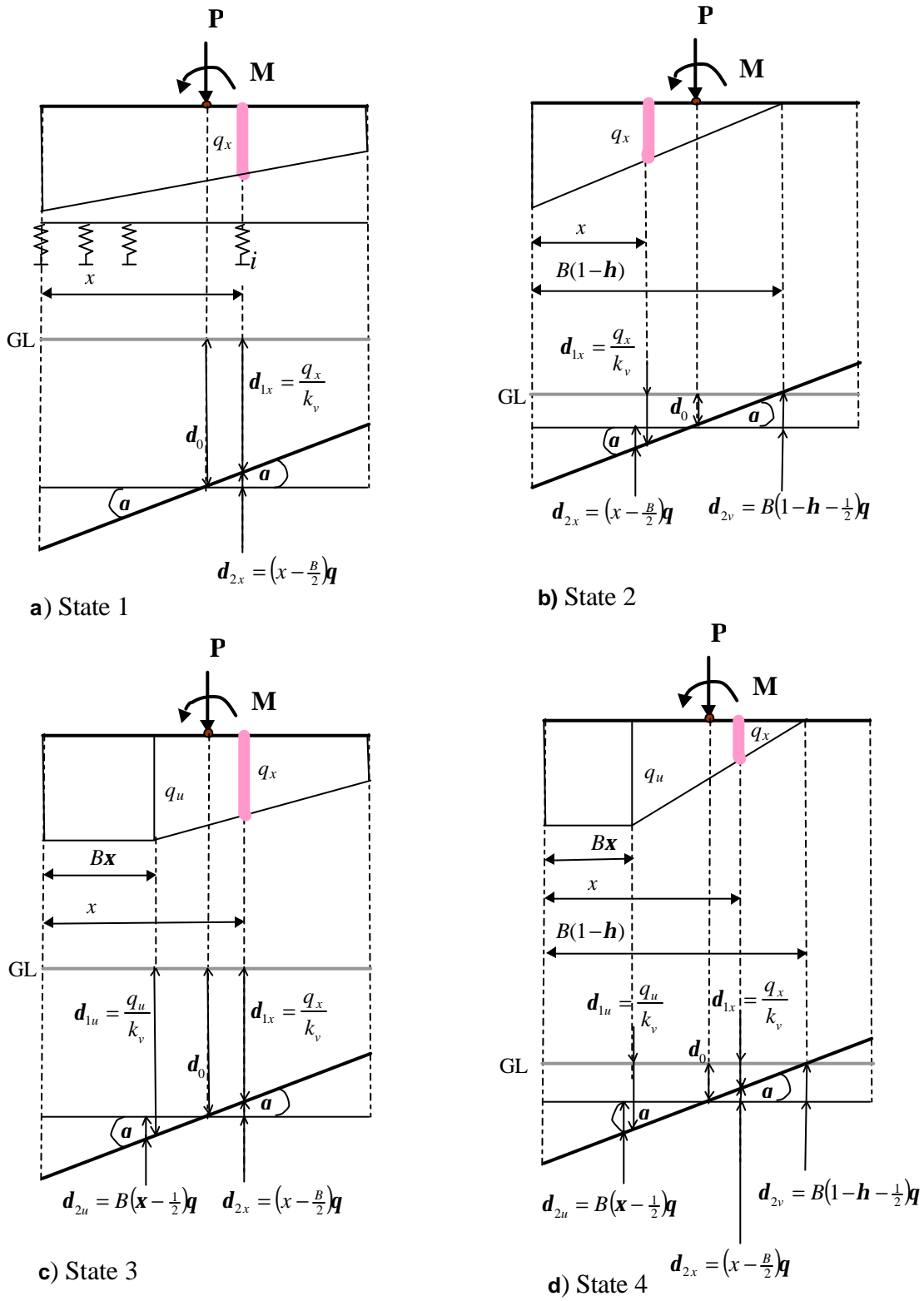


Figure II.1 Stresses and displacements for different footing states

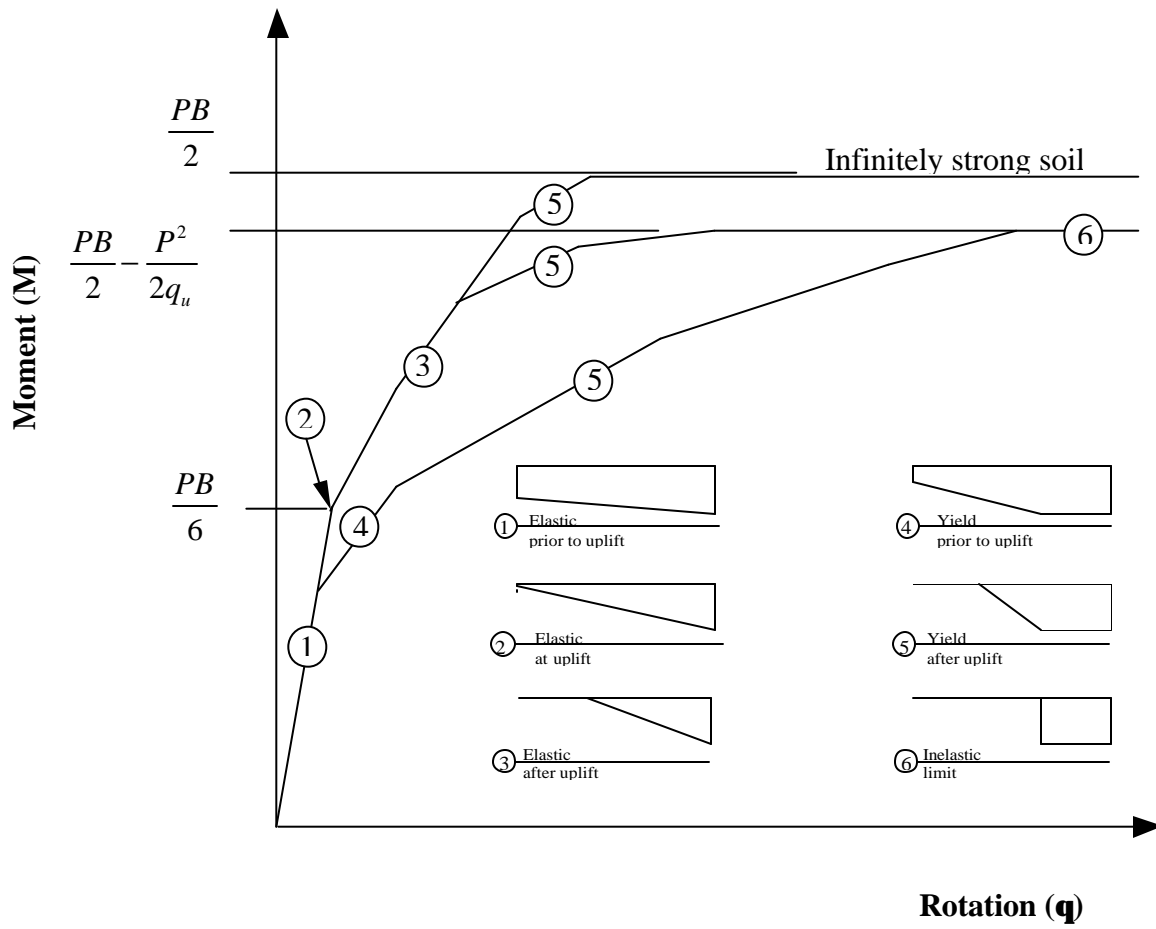
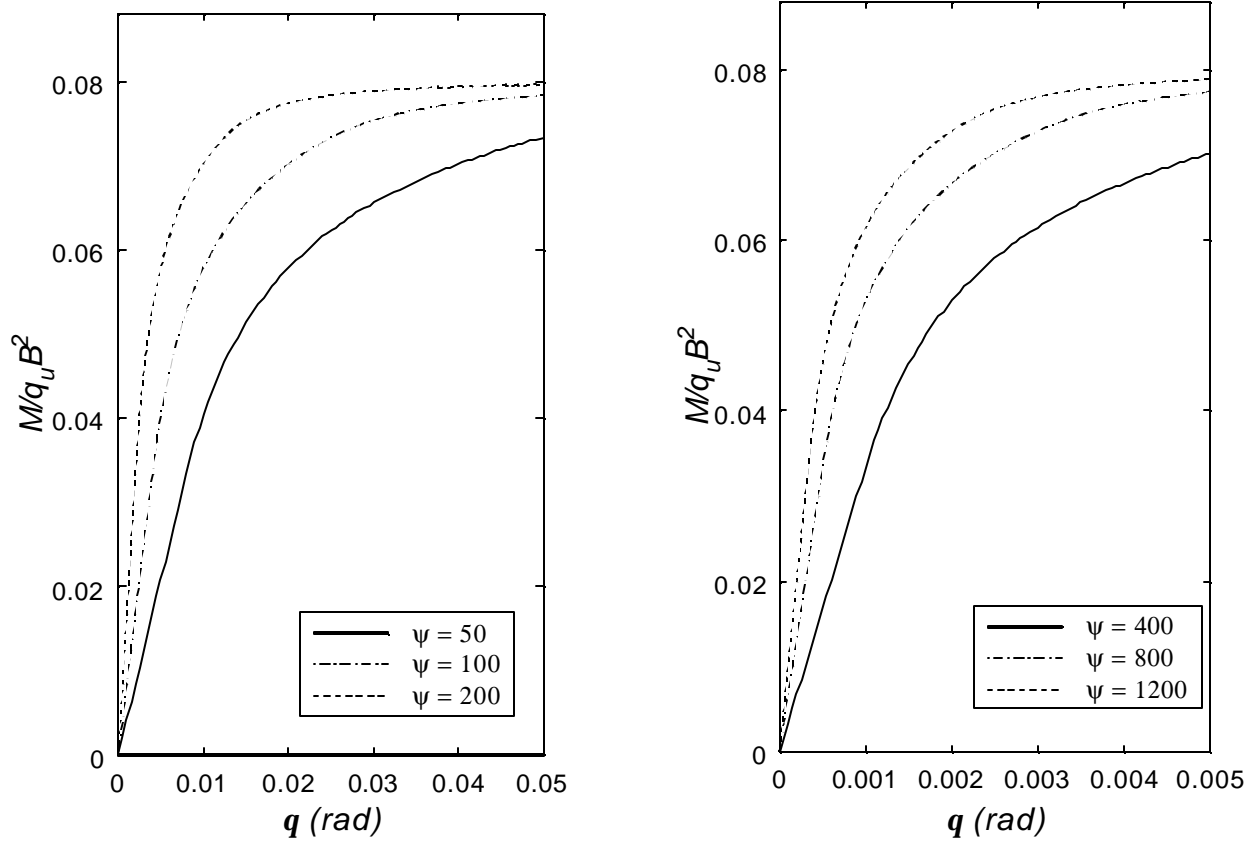


Figure II.2 Schematic of different states of moment-rotation response (after FEMA 273/274)

Figure II.3 Computed moment-rotation curves for $c = 0.2$ a) for small \mathbf{y} ; b) large \mathbf{y}



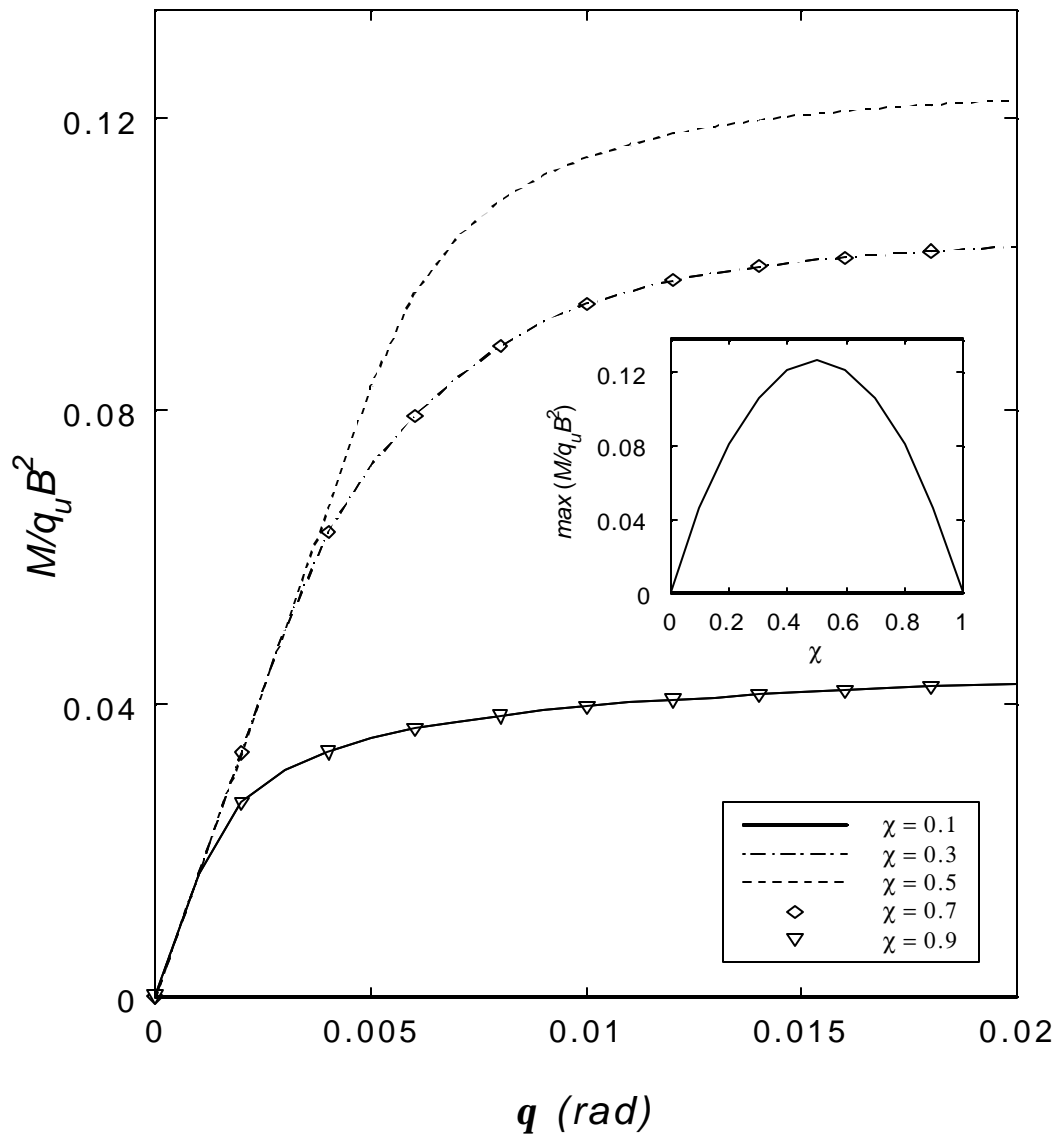


Figure II.4 Computed moment-rotation curves for different values of \mathbf{c} for $\mathbf{y} = 200$

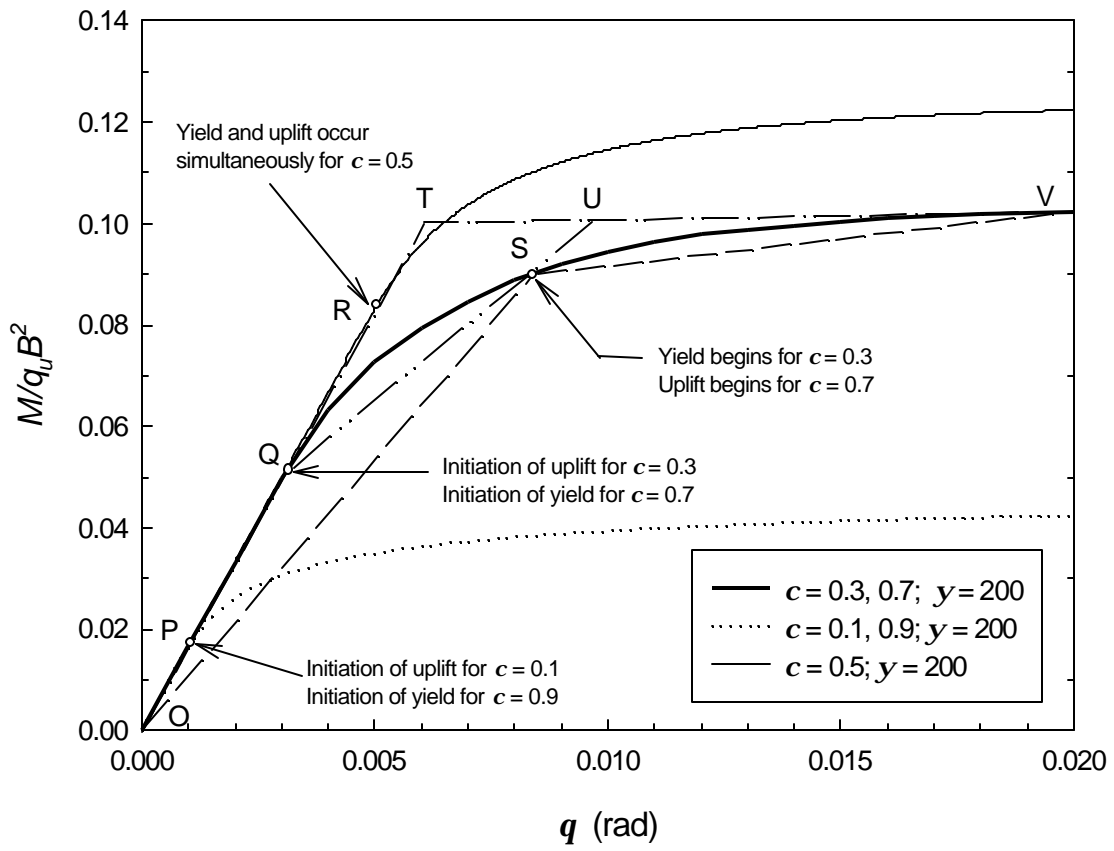


Figure II.5 Computed moment-rotation curves showing points of change of state

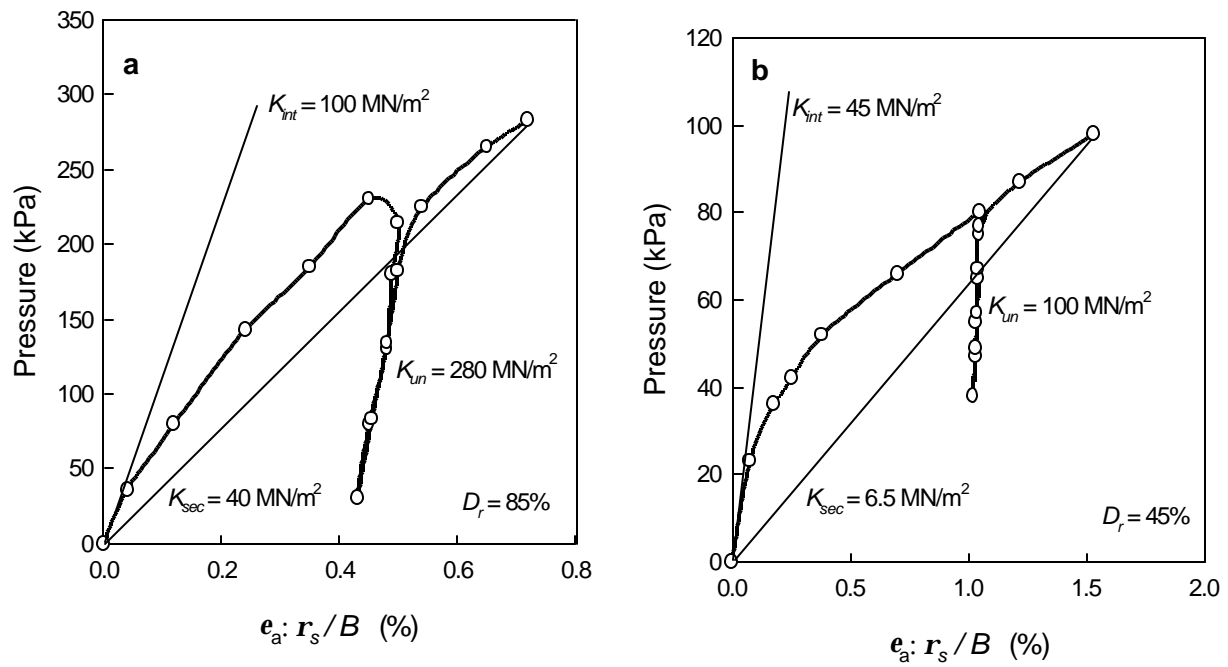


Figure II.6 Load-deformation results from TRISEE experiments: a) load-deformation curves for HD tests; b) load-deformation curves for LD tests

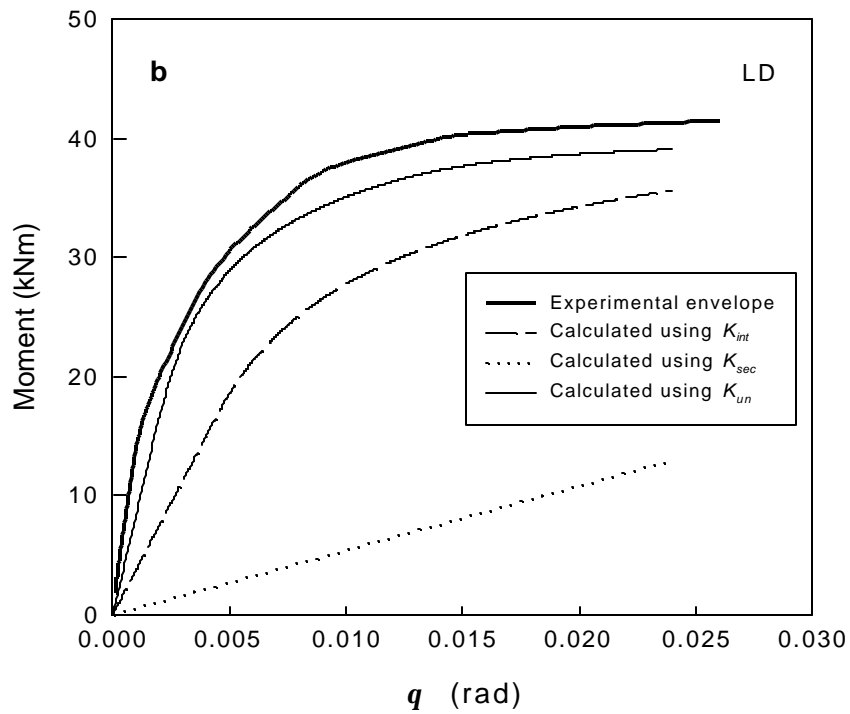
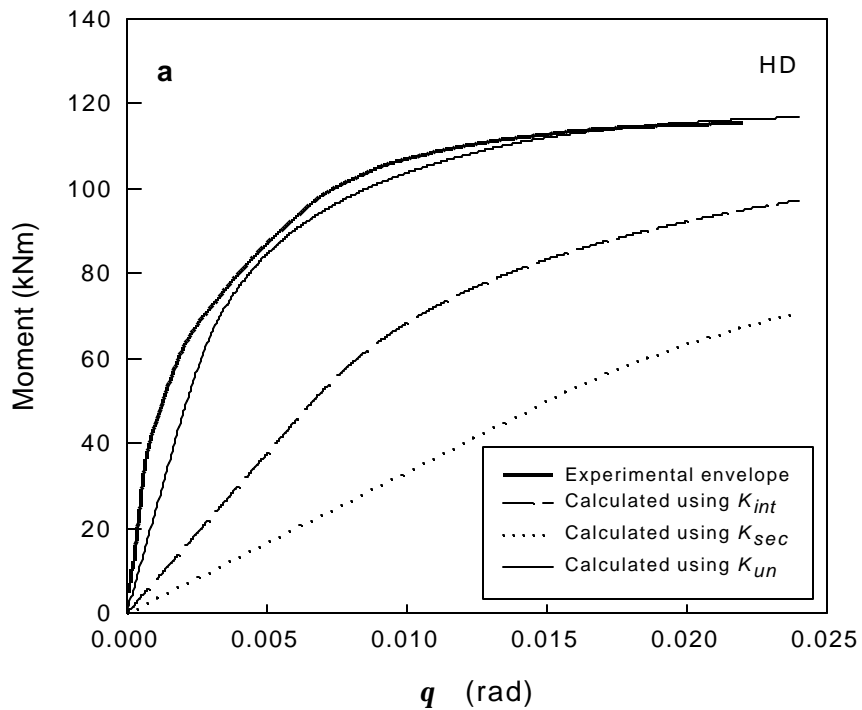


Figure II.7 Comparison between predicted and experimental moment-rotation curves